Range correlation and I/Q performance benefits in single-chip silicon Doppler radars for noncontact cardiopulmonary monitoring

5 Author(s)

A.D. Droitcour ; O. Boric-Lubecke ; V.M. Lubecke ; J. Lin ; G.T.A. Kovacs

View All Authors

Abstract:
Direct-conversion microwave Doppler-radar transceivers have been fully integrated in 0.25-/spl mu/m silicon CMOS and BiCMOS technologies. These chips, operating at 1.6 and 2.4 GHz, have detected movement due to heartbeat and respiration 50 cm from the subject, which may be useful in infant and adult apnea monitoring. The range-correlation effect on residual phase noise is a critical factor when detecting small phase fluctuations with a high-phase-noise on-chip oscillator. Phase-noise reduction due to range correlation was experimentally evaluated, and the measured residual phase noise was within 5 dB of predicted values on average. In a direct-conversion receiver, the phase relationship between the received signal and the local oscillator has a significant effect on the demodulation sensitivity, and the null points can be avoided with a quadrature (I/Q) receiver. In this paper, measurements that highlight the performance benefits of an I/Q receiver are presented. While the accuracy of the heart rate measured with the single-channel chip ranges from 40% to 100%, depending on positioning, the quadrature chip accuracy is always better than 80%.

Published in: IEEE Transactions on Microwave Theory and Techniques (Volume: 52, Issue: 3, March 2004)

Page(s): 838 - 848

Date of Publication: 15 March 2004

ISSN Information:

INSPEC Accession Number: 8004126

DOI: 10.1109/TMTT.2004.823552

Publisher: IEEE

Sponsored by: IEEE Microwave Theory and Techniques Society

SECTION I.
Introduction

MICROWAVE Doppler radar has been used to sense physiologic movement since the early 1970s [1]. The original work was done with bulky, heavy, and expensive waveguide components, but recent advances in wireless technologies have made it feasible to integrate such a radar on a single chip [2], [3], which is compact, lightweight, and could be inexpensively mass-produced. With less expensive and smaller circuitry, microwave Doppler radar could potentially be used in home monitoring, particularly for sleep apnea in both infants and adults, where long-term monitoring using chest straps is often prescribed [4], [5]. Obstructive sleep apnea syndrome (OSAS) affects 4% of all adult males and has many symptoms, including hypertension, psychological distress, and cognitive impairment [6]. Although rates of sudden infant death syndrome (SIDS) have declined sharply in the past ten years, SIDS is still the third leading cause of infant mortality [7], and many more infants suffer from apnea [4]. Microwave Doppler monitoring offers a noncontact alternative to commonly prescribed chest-strap monitors and, therefore, may provide a less intrusive option.

Doppler-radar motion-sensing systems typically transmit a continuous-wave (CW) signal

(sometimes frequency modulated), which is reflected off a target and then demodulated in the receiver. According to Doppler theory, a target with a time-varying position, but a net zero velocity, will reflect the signal with its phase modulated proportionally to the time-varying target position. A stationary person's chest has a periodic movement with a net zero velocity, and therefore, a CW radar with the chest as the target will receive a signal similar to the transmitted signal with its phase modulated by the time-varying chest position. Demodulating the phase will then give a signal directly proportional to the chest position, which contains information about movement due to heartbeat and respiration, from which heart and respiration rates and signatures can be determined. Based on this principle, a noncontact heart and respiration monitor can be envisioned. By leveraging existing wireless technology, it would be possible to manufacture an inexpensive and portable device to perform such monitoring.

Microwave Doppler radar was first applied to the measurement of respiration rate and the detection of apnea in 1975 [1]. Starting in the early 1980s, similar systems were proposed to search for victims trapped in earthquake rubble or an avalanche [8] and to sense human presence behind a wall or other barrier [9]. All of these systems used bulky heavy microwave components and large antennas, which are acceptable for use in diagnostic or emergency situations, but are impractical for everyday home monitoring. Other options for home monitoring of heart and respiration rates are the Polar strap for heart monitoring [10], straps that measure chest expansion, such as Respitrace [11], for respiration monitoring, acoustic monitors, nasal/oral airflow sensors, and pulse oximetry. While all of these require contact with the body, and most require careful placement, a single-chip Doppler radar may provide a more flexible noncontact alternative.

The silicon radar chips presented in this paper are direct-conversion Doppler radars, operating at 1.6 and 2.4 GHz, each with a single oscillator and output power comparable to the low-end power of consumer electronics (under 10 mW). The 2.4-GHz radar uses a quadrature (I/Q) receiver in order to avoid null points [9] and, thus, improve upon the accuracy of 1.6-GHz radars described in [2] and [12]. One of the challenges involved in using a silicon CMOS radar is the translation of oscillator phase noise, notoriously high in fully integrated CMOS oscillators, to output amplitude noise. When the same source is used for transmitting and receiving, the phase noise of the received signal is correlated with that of the local oscillator (LO), with the level of correlation dependent on the time delay between the two signals. When the delay is small, this effect greatly decreases the noise spectrum at baseband. For example, at a 50-cm range, the baseband noise at 10 Hz is 134 dB below the RF phase noise [2]. In a radar application, this time delay is proportional to the target range. Hence, this phase-noise-reducing effect is known as range correlation [13]. Range correlation is particularly important in measuring chest-wall movement since the heart and respiration information is encoded in phase modulations of 0.1–10 Hz, where the phase noise is near its peak [2].

This paper will present two important aspects of single-chip Doppler-radar performance: range-correlation phase-noise filtering and the performance benefits of a quadrature receiver architecture. Both effects are evaluated experimentally. A Doppler-radar architecture that takes advantage of these effects is described, and both single-channel and quadrature silicon radar chips are tested for comparison. Measured residual phase noise at baseband agreed with range-correlation theoretical values within an average of 5 dB, and the effects of phase-noise and range correlation on heart-rate detection accuracy are evaluated. Radar chips placed near the optimum phase-demodulation point and at approximately a 50-cm range detected a heart rate within one beat per minute of corresponding wired reference signals for over 98% of the measurement interval. The use of a quadrature receiver improved the lowest accuracy, which occurs at the phase-demodulation null point, from 40% to 80%.

SECTION II.
Quadrature Doppler Radar and Range-Correlation Theory

Neglecting amplitude variations, a CW radar typically transmits a single-tone signal

$$T(t) = \cos\left(2\pi f t + \phi(t)\right) \tag{1}$$

View Source

where f is the oscillation frequency, t is the elapsed time, and $\phi(t)$ is the phase noise of the oscillator. If this signal is reflected by a target at a nominal distance d_0 with a time-varying displacement given by $x(t)$, the total distance traveled between the transmitter and receiver is $2d(t) = 2d_0 + 2x(t)$. The received signal can be found as

$$R(t) = \cos\left[2\pi f\left(t - \frac{2d\left(t - \frac{d(t)}{c}\right)}{c}\right) + \phi\left(t - \frac{2d\left(t - \frac{d(t)}{c}\right)}{c}\right)\right] \quad (2)$$

View Source

where c is the signal's propagation velocity. Substituting for $d(t)$, and expanding, the received signal is

$$R(t) = \cos\left[2\pi f t - \frac{4\pi d_0}{\lambda} - \frac{4\pi x\left(t - \frac{d(t)}{c}\right)}{\lambda} + \phi\left(t - \frac{2d_0}{c} - \frac{2x\left(t - \frac{d(t)}{c}\right)}{c}\right)\right] \quad (3)$$

View Source

where the wavelength is $\lambda = c/f$. Assuming that the $d(t)/c$ term in $x(t - d(t)/c)$ is negligible because the chest moves with a period $T \gg d_0/c$, and assuming that the $x(t - d(t)/c)/c$ term is negligible in the phase-noise term, since $x(t) \ll d_0$, the received signal can be approximated as

$$R(t) \approx \cos\left[2\pi f t - \frac{4\pi d_0}{\lambda} - \frac{4\pi x(t)}{\lambda} + \phi\left(t - \frac{2d_0}{c}\right)\right]. \quad (4)$$

View Source

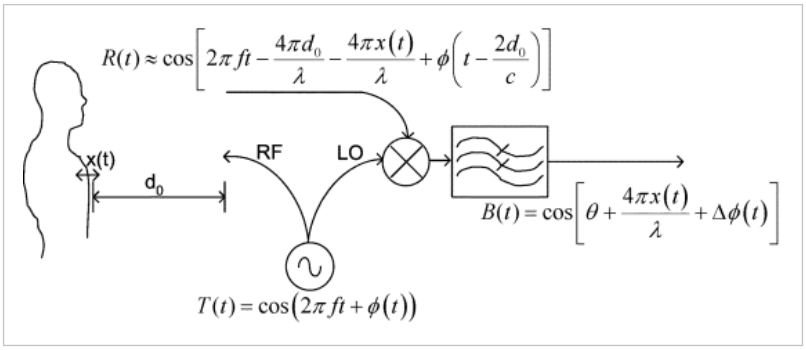

Fig. 1. Simplified Doppler-radar system block diagram with signal flow. The target, at a nominal distance from the antenna d_0 has a periodic displacement $x(t)$. The oscillator signal $T(t)$ provides both the transmitted RF signal and the LO. The transmitted signal travels a total distance $2d(t) = 2d_0 + 2x(t)$ and becomes the received signal $R(t)$, which is mixed with the LO and low-pass filtered to give the baseband output $B(t)$.

The received signal is similar to the transmitted signal with a time delay determined by the nominal distance of the target and with its phase modulated by the periodic motion of the target. The information about the periodic target motion can be demodulated if this signal is multiplied by an LO signal that is derived from the same source as the transmitted signal. This radar topology takes advantage of the ability to use the same oscillator for the transmitter and LO, which keeps the phase noise of the two signals correlated.

When the received and LO signals are mixed and the output is low-pass filtered, the resulting baseband signal is

$$B(t) = \cos\left[\theta + \frac{4\pi x(t)}{\lambda} + \Delta\phi(t)\right] \quad (5)$$

View Source

where

$$\Delta\phi(t) = \phi(t) - \phi\left(t - \frac{2d_0}{c}\right) \quad (6)$$

$$\Delta\varphi(t) = \varphi(t) - \varphi\left(t - \frac{2d_0}{c}\right) \quad (6)$$

View Source

is the residual phase noise and

$$\theta = \frac{4\pi d_0}{\lambda} + \theta_0 \quad (7)$$

View Source

is the constant phase shift dependent on the nominal distance to the target d_0. Several factors affect the value of θ_0 such as the phase shift at the reflection surface (near 180°) and any distance between the mixer and antenna. Fig. 1 shows a simplified block diagram and the signal flow of a Doppler-radar system used to detect periodic target motion.

If θ in (7) is an odd multiple of $\pi/2$, the small-angle approximation is valid for $x(t) \ll \lambda$ and the baseband output is approximately

$$B(t) \approx \frac{4\pi x(t)}{\lambda} + \Delta\phi(t). \quad (8)$$

View Source

In this case, the optimum phase-demodulation sensitivity is achieved and the baseband output is proportional to the periodic chest displacement $x(t)$ summed with the residual phase noise.

When θ is an integer multiple of π, the output is approximately

$$B(t) \approx 1 - \left[\frac{4\pi x(t)}{\lambda} + \Delta\phi(t)\right]^2. \quad (9)$$

View Source

In this case, the baseband output is no longer linearly proportional to the time-varying displacement, and the sensitivity is decreased. This null point occurs when the LO $T(t)$ and received signal $R(t)$ are either in-phase or 180° out-of-phase. Since the variable part of θ is dependent only on the distance to the target d_0, this null point occurs with a target distance every $\lambda/4$ from the radar. At a frequency of 2.4 GHz, these null points occur every 3 cm and therefore can be difficult to avoid by adjusting the position of the transceiver. These null points can be avoided with a quadrature receiver, where two receiver chains, with LO phases $\pi/2$ apart, insure that there is always at least one output not in the null point.

With a quadrature receiver, the two receiver output channels will be

$$B_I(t) = \cos\left[\theta + \frac{\pi}{4} + \frac{4\pi x(t)}{\lambda} + \Delta\phi(t)\right] \quad (10)$$

View Source

and

$$B_Q(t) = \cos\left[\theta - \frac{\pi}{4} + \frac{4\pi x(t)}{\lambda} + \Delta\phi(t)\right]. \quad (11)$$

View Source

When $\theta + \pi/4$ is an integer multiple of π, the I signal will be in the null point (9). However, $\theta - \pi/4$ will be an odd multiple of $\pi/2$ and the Q signal will be in the optimum phase-demodulation point (8). With a quadrature receiver, the worst case is when θ is an integer multiple of π so both $\theta + \pi/4$ and $\theta - \pi/4$ are odd multiples of $\pi/4$, and neither receiver chain is at the optimum phase-demodulation point. At this point, the baseband outputs are

$$B_I(t) = B_Q(t) \approx \frac{1}{\sqrt{2}} - \frac{1}{\sqrt{2}} \cdot \left[\left(\frac{4\pi x(t)}{\lambda} + \Delta\phi(t)\right) + \frac{1}{2}\left(\frac{4\pi x(t)}{\lambda} + \Delta\phi(t)\right)^2\right]. \quad (12)$$

View Source

As long as $x(t) \ll \lambda$, the linear term is much larger than the squared term, and the heart signal can still be detected.

Range-correlation theory describes how the residual phase noise, $\Delta\phi(t)$ in (5)–(12), affects the baseband noise spectrum, and it was first proposed to explain why CW radar systems were not swamped by ground clutter noise [14]. According to [13], with the target at a given range R, the baseband noise spectral density at offset frequency f_o is as follows in (13), where the RF phase-noise density is $S_\phi(f)$:

$$S_{\Delta\phi}(f_o) = S_\phi(f_o)\left[4\sin^2\left(2\pi\frac{Rf_o}{c}\right)\right]. \tag{13}$$

View Source

At values relevant for radar monitoring of heart and respiration, Rf_o/c will be on the order of 10^{-9}, so the small-angle approximation is valid and range correlation will cause the baseband noise spectrum to increase proportionally to the square of the target range R and the square of the offset frequency f_o:

$$S_{\Delta\phi}(f_o) \approx S_\phi(f_o)\left[16\pi^2\frac{R^2{f_o}^2}{c^2}\right]. \tag{14}$$

View Source

For example, with a 50-cm range and an offset frequency of 1 Hz, the value of Rf_o/c is 1.67×10^{-9}. The error due to the small-angle approximation at this point is near 10^{-60}.

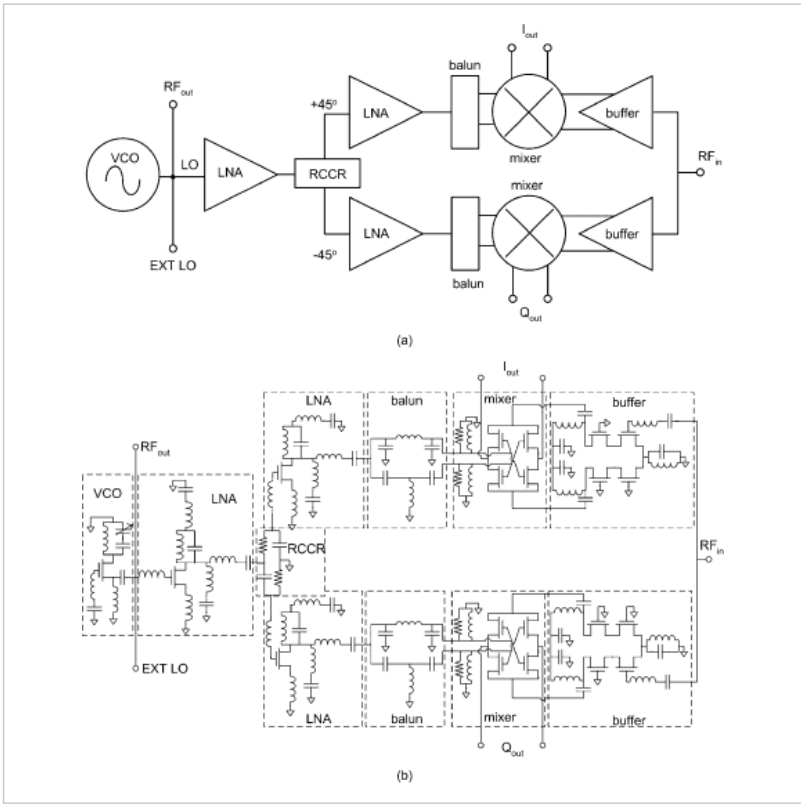

Fig. 2. (a) Block diagram and (b) simplified circuit diagram (with biasing not shown) of the quadrature transceiver.

Since the close-in RF phase-noise spectrum of an oscillator has a -30-dB/decade slope, and it is effectively attenuated by a filter with a $+20$-dB/decade slope, the resulting baseband noise spectrum is expected to have a -10-dB/decade slope. For a 50-cm range and an offset frequency of 1 Hz, the residual phase noise is decreased by 154 dB. Range correlation has a much less significant effect on amplitude noise. For small Rf_o/c and Gaussian white amplitude noise, it results in a gain of 3 dB [13]. Since, as shown in (8), the residual phase noise appears as additive noise on the baseband signal, the phase-noise reduction due to the range-correlation effect is particularly important. If two different oscillators with uncorrelated phase noise were used for transmitting and receiving, it would be impossible to detect the small phase variations created by heart and respiration motion.

Based on subcircuits developed for BiCMOS and CMOS DCS1800/PCS1900 base-station receiver chips [15]–[16][17], single-chip radar transceivers were designed at 1.6 and 2.4 GHz. A block diagram, simplified circuit diagram, and micrograph of the nonquadrature radar transceiver are shown in [2] and the block diagram and simplified circuit diagram of the quadrature radar transceiver are shown in Fig. 2(a) and (b), respectively, whereas its micrograph can be found in [3]. These chips follow the basic Doppler-radar architecture shown in Fig. 1. As shown in Fig. 2, the quadrature chip uses two identical receiver chains to provide quadrature outputs. The $\mathrm{RF}_{\mathrm{out}}$ and LO signals from the voltage-controlled oscillator (VCO) are split without using a balun. The LO is amplified with a low-noise amplifier (LNA) and is then split with an resistor–capacitor–capacitor–resistor (RC–CR) circuit into two quadrature LO signals for the in-phase (I) and quadrature (Q) receiver chains. Another LNA amplifies each of these signals to provide isolation between the I and Q LOs, and a passive LC balun transforms each single-ended LO into the differential LO required by the double-balanced mixer. The RF input is split in two for I and Q channels, and active baluns provide differential RF signals to feed the mixer. The two quadrature outputs help to avoid the phase-demodulation null points, as shown in (9).

SECTION III.
Range-Correlation Evaluation

The effect of range correlation on baseband residual phase noise for different offset frequencies and time delays was estimated using (13) and phase-noise data obtained for the quadrature chip [3]. The range-correlation theory was verified by varying the delay between the transmitter and the receiver and measuring the baseband noise spectrum at the I or Q output and comparing it with the predicted values. The setup of this experiment is shown in

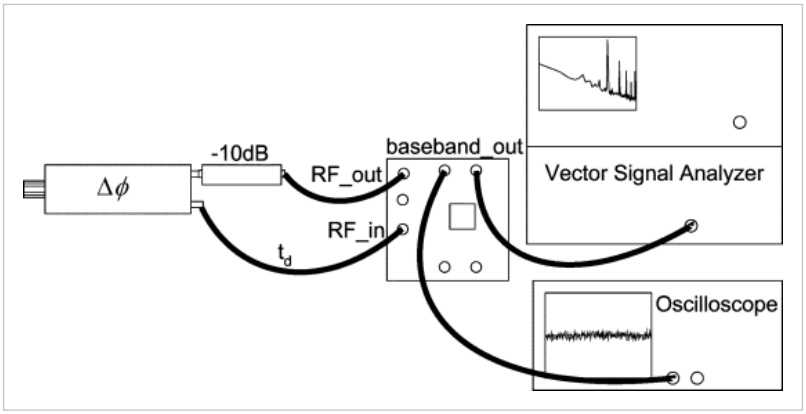

Fig. 3. Setup for the range-correlation verification experiment. The baseband noise spectrum was measured with the VSA. Cables of various lengths were connected in the place of the cable marked t_d to change the time delay between the RF and LO signals.

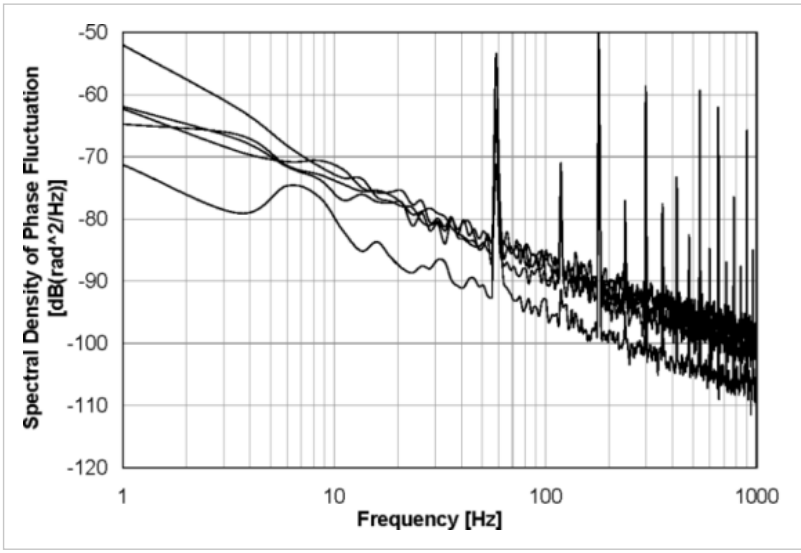

Fig. 4. Baseband noise spectrum measured for various phase shifts with a 20.9-ns time delay. When the two signals are near in-phase or out-of-phase, the dc voltage at the output is nonzero, and the phase-demodulation sensitivity is greatly decreased.

Fig. 3. The RF output of the chip was connected to the phase-shifter input through a 30-cm SMA

cable and a 10-dB attenuator. The 10-dB attenuator was used to reduce VCO loading by the phase shifter. An SMA cable connected the phase-shifter output to the RF input of the chip. The length of this cable, marked t_d in Fig. 3, was varied to change the time delay between the RF and LO signals. The baseband output of the chip was measured with an HP89410A vector signal analyzer (VSA). To ensure consistent measurements, the RF and LO signals were kept in quadrature (θ in (7) is an odd multiple of $\pi/2$) so the maximum phase-to-voltage sensitivity is maintained. To find this point, a Pasternack phase shifter (PE8442) was used to tune the phase relationship until the dc component of the baseband signal, as viewed on an oscilloscope,

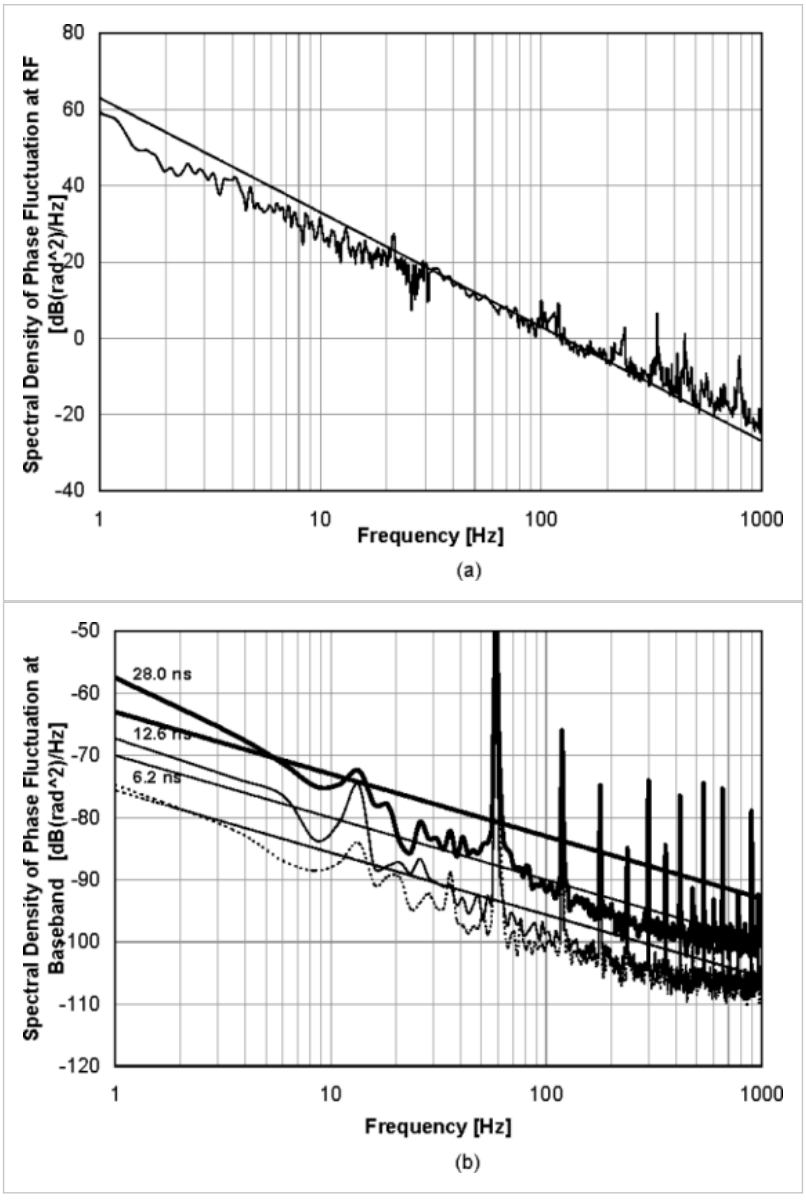

Fig. 5. (a) Measured phase noise at RF and -30-dB/decade line used to predict baseband phase noise. (b) Measured and predicted (13) spectral density of phase fluctuation at baseband for time delays of 28.0, 12.6, and 6.2 ns (from top to bottom).

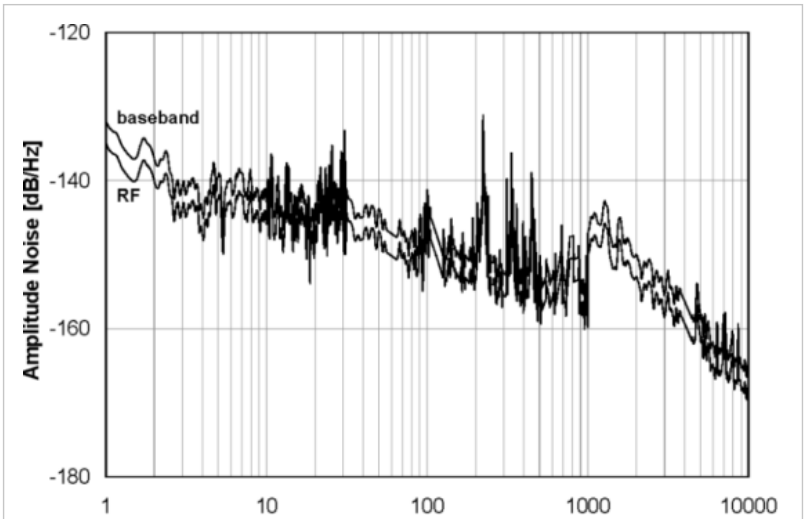

Frequency [Hz]

Fig. 6. Measured oscillator amplitude noise (RF), shown with predicted baseband amplitude noise.

was zero. All unused RF connectors were terminated with 50-Ω loads. The baseband noise spectrum from 1 Hz to 1 kHz was measured with a 1-Hz resolution bandwidth and rms averaged over five measurements. The baseband noise spectrum measurements were converted to a phase-noise equivalent by calculating the ratio of the measured noise power to the power a 30-kHz IF signal would have with the same RF and LO power. This was then converted to spectral density of phase fluctuation $S_{\Delta\phi}(f)$ by multiplying by two [18]. The time delay and loss through the cables, attenuator, and phase shifter were measured with an HP 8714C RF network analyzer, and the loss was taken into account when calculating the equivalent IF power.

To show the importance of tuning the phase relationship so the RF and LO signals are in quadrature, the baseband noise plots are shown with the phase tuned to different positions in Fig. 4. When the RF and LO signals are either in-phase or 180° out-of-phase, the phase-demodulation sensitivity is reduced, and the residual phase noise can appear much lower than it does when the signals are in quadrature. In order to compare results for various time delays in range-correlation measurements, it was important to ensure that all measurements were made at the optimum phase-sensitivity demodulation point (8). It may seem that using this effect to decrease the residual phase noise would be beneficial. However, since the chest motion is encoded as a phase modulation, as the phase-to-voltage sensitivity decreases, the baseband signal will decrease with the noise, and no benefit can be derived from this effect. Fig. 4 also shows that the measurement in the 1–10-Hz decade was very noisy. The measurements selected for the range-correlation verification were chosen based on a slope that was consistent with the rest of the data. The variation in the power spectral density of the traces with dc values near zero was within the error for any individual measurement.

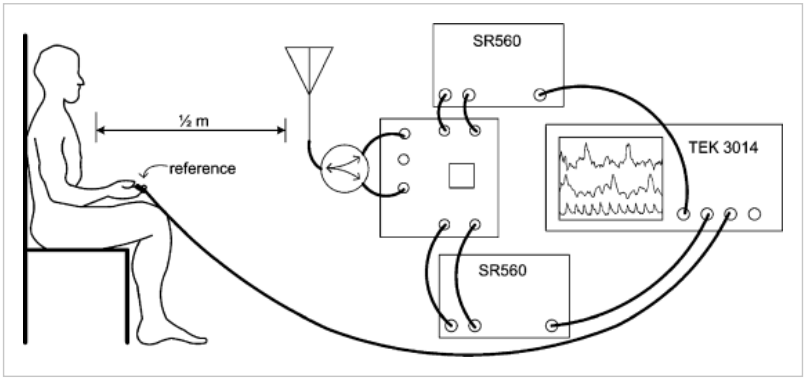

Fig. 7. Heart and respiration activity measurement setup. The baseband output signals were amplified and filtered with SR560 LNAs and then digitized with a Tektronix 3014 digital oscilloscope. A wired finger-pressure pulse sensor was used only as a reference to compare to the heart-rate data obtained with the Doppler radar.

The measured phase noise and the -30-dB/decade slope line used to predict the baseband noise are shown in Fig. 5(a) for offset frequencies from 1 Hz to 1 kHz. The predicted and measured phase fluctuation spectral density are plotted in Fig. 5(b) for delays of 6.2, 12.6, and 28.0 ns, and offset frequencies from 1 Hz to 1 kHz. On average, the measured values were within 5 dB of the predicted values. The baseband phase noise was reduced by 148 to 136 dB at 1 Hz for the time delays from 6.2 to 28.0 ns, which correspond to ranges from 0.93 to 4.2 m. The measured baseband noise spectral density was in the same range as predicted based on the previously measured phase noise and range-correlation theory. The measured baseband noise increased as the time delay increased and had approximately a -10-dB/decade slope, as was predicted. Some variation in the measurement may be due to the RF and LO signals not being exactly in quadrature and affecting the phase-demodulation sensitivity (Fig. 4). The phase noise was not measured at the same time as the baseband noise spectrum, and this may be another cause for some of the discrepancy between the predictions and measured results.

The amplitude noise of the oscillator, measured with the HP E5500 system, is shown in Fig. 6, along with the predicted amplitude noise at baseband after range correlation [13]. Amplitude noise was under -130 dB/Hz and, therefore, below the phase noise for frequencies under 10 kHz, even after range correlation. Since the amplitude noise is significantly lower than the phase noise for all frequencies of interest, it does not affect the accuracy of heart-rate measurements.

SECTION IV.

Heart and Respiration Activity Measurements

To assess I/Q performance enhancement, as well as performance difference due to varying levels of residual phase noise, vital signs data were collected with the following three chips:

1.6-GHz single-channel BiCMOS chip;

1.6-GHz single-channel CMOS chip;

2.4-GHz quadrature CMOS chip

with similar output power, under 10 mW. Fig. 7 shows the experimental setup used to make measurements with the 2.4-GHz industrial–scientific–medical (ISM) band quadrature chip. A Mini-Circuits power splitter, part ZAPD-4, provided 17 dB of isolation between the input and output signals, and a commercially available Antenna Specialists ASPPT2988 2.4-GHz ISM-band patch antenna with 60° × 80° beamwidth was used. The subject was seated approximately 50 cm from the antenna, fully clothed, facing the antenna, and breathing normally. A wired finger-pressure pulse sensor (UFI_1010 pulse transducer) was used during the measurements to provide a reference signal for heart activity. The baseband output was filtered with Stanford Research Systems model SR560 LNAs using 0.1-Hz high-pass and 10-Hz low-pass analog filters, each with a 12-dB/decade slope, and a total gain of 33 dB to remove dc offset and avoid aliasing. Although the high-pass analog filter reduces the amplitude of the respiration signal, the respiration rate can still be extracted since the respiration signal amplitude is significantly larger than the heart signal amplitude. The resulting waveforms were digitized with a Tektronix 3014 digital oscilloscope. The digitized signals were processed to determine the

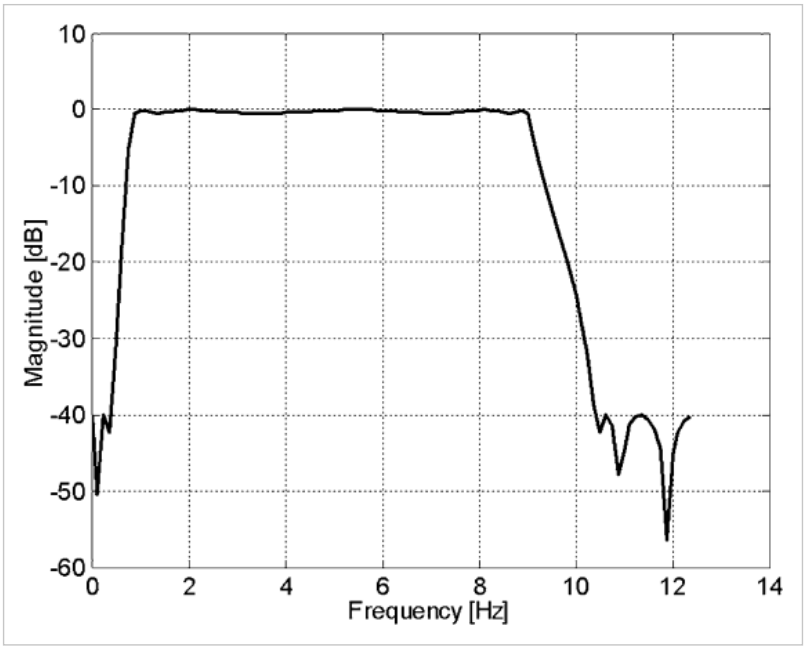

Fig. 8. Frequency response of the twelfth-order elliptic IIR filter used to separate the heart signal from the signal that includes both heart and respiration information. The fundamental frequency of respiration is usually below 0.4 Hz, while the heart rate is usually above 1 Hz.

heart and respiration rates over time. The heart-rate accuracy was calculated as the percentage of the measurement interval that the heart rate measured with the Doppler radar was within one beat per minute of the rate measured with the wired reference.

A. I/Q Performance Assessment

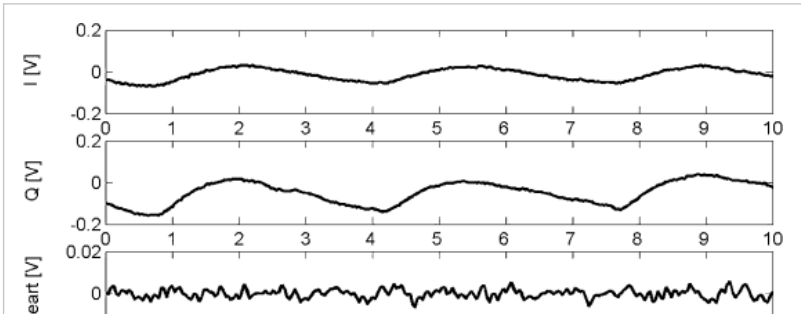

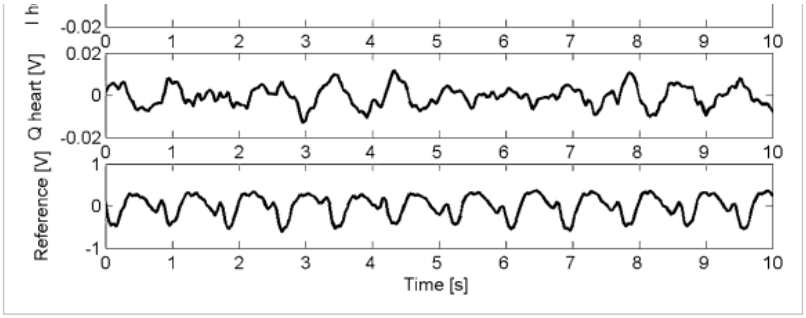

Fig. 9. Heart and respiration activity measured with the 2.4-GHz quadrature chip. The analog-filtered I and Q outputs, which contain both heart and respiration information, are shown at the top, followed by the digitally filtered I and Q signals, with only heart information. Neither the I, nor Q, output is at the maximum sensitivity point or at the null point. Their amplitudes and accuracies are similar. The I output is within one beat per minute of the reference 82% of the time, and the Q output is correct 81% of the time.

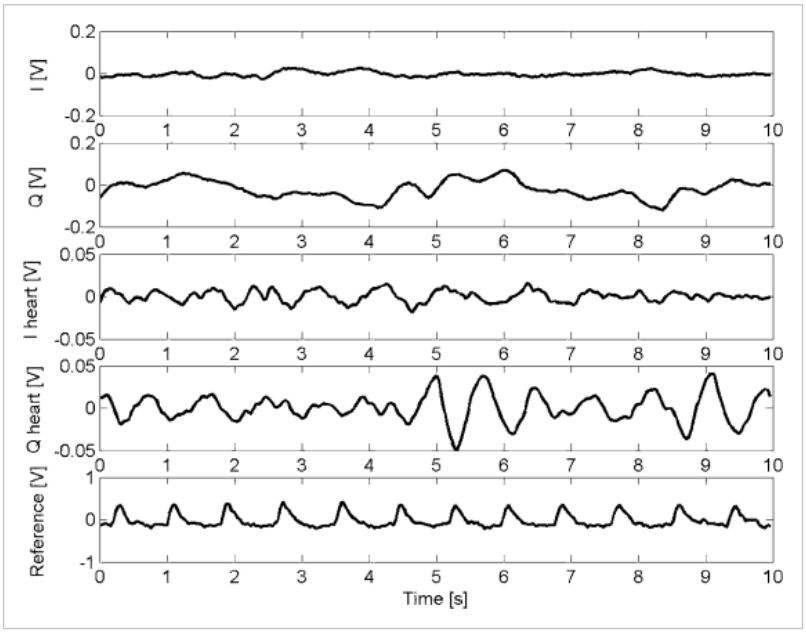

Fig. 10. Heart and respiration activity measured with the 2.4-GHz quadrature chip. The analog-filtered I and Q outputs are shown at the top, followed by the digitally filtered I and Q signals. The Q output is near the maximum sensitivity point and the I signal is near the null point so the amplitude of the Q signal is greater than that of the I signal. The I output is within one beat per minute of the reference 46% of the time and the I output 100% of the time.

The heart and respiration signals were separated with a MATLAB script using techniques similar to those given in [19]. Both the I and Q signals were digitally filtered with a twelfth-order elliptic infinite impulse response (IIR) bandpass filter, which passed 0.9–9 Hz, blocking frequencies below 0.8 Hz, as shown in Fig. 8. The signals were windowed and then autocorrelated, and the fast fourier transform (FFT) of the autocorrelated signal was calculated in each window. The heart rate was calculated from the frequency where this FFT had its maximum. Respiration rates were obtained using a similar method, without the digital filtering, and with a larger window.

In Figs. 9 and 10, data collected using the ISM-band quadrature transceiver is shown. In Fig. 9, neither output is in quadrature for maximum phase sensitivity or in the null point for the worst phase sensitivity (12). The Doppler-radar system determined a heart rate of 70 beats per minute, which is within one beat per minute of the rate determined with the wired reference for 82% of the measurement interval in the Q signal, and 81% of the interval in the I signal. The respiration rate is 18 breaths per minute. In Fig. 10, the I trace is near the phase-demodulation null point (9), while the Q trace is near the optimum phase-demodulation point (8). In this signal, the I signal matches the reference, also at 70 beats per minute, 46% of the time, while the Q signal matches 100% of the time. These measurements illustrate the benefit of the I/Q receiver over a single-ended receiver in the worst case measurements. The worst case with a single-ended receiver would be 46% in the null point, while with the quadrature receiver, the worst case is 81% at a point between the null and optimum points.

B. Effects of Varying Residual Phase Noise

TABLE I Summary of the Heart-RateDetection MeasurementAccuracy. Below the Accuracy Percentage, the Estimated Phase-Demodulation Null Point is Listed: "Opt" Indicates the Optimum Point (8), "Null" Indicates the Null Point (9), and "Mid" Indicates a Point Between the Optimum and Null (12)

Fig	Chip	Fit Measured Phase Noise $S_\phi(f)$ [dB/Hz]		Target Range [cm]	Predicted Baseband Noise $S_{\Delta\phi}(f)$[dB/Hz]		Quadrature		Non-quadrature	
		1Hz	10Hz		1Hz	10Hz	I%	Q%	Raw%	Heart%
10	2.4GHz CMOS	+64	+33	50cm	-90	-102	82 mid	81 mid	—	—
11	2.4GHz CMOS	+64	+33	50cm	-90	-102	46 null	100 opt	—	—
12	1.6GHz BiCMOS	+52	+21	50cm	-102	-113	—	—	92 opt	100 opt
13	1.6GHz CMOS	+64	+33	50cm	-90	-102	—	—	85 opt	98 opt
14	1.6GHz CMOS	+64	+33	50cm	-90	-102	—	—	33 null	44 null
15	1.6GHz CMOS	+64	+33	85cm	-85	-97	—	—	52 opt	63 opt

To show the effects of varying residual phase noise on signal quality, signals obtained with chips with different levels of oscillator phase noise and with the target at a varying range were examined. The phase noise and predicted residual phase noise at 1- and 10-Hz offsets are shown for each trace in Table I. The phase noise from the 1.6-GHz CMOS chip [2] and the 2.4-GHz CMOS chip [see Fig. 5(a)] were similar, while the phase noise from the 1.6-GHz BiCMOS chip with a bipolar VCO was approximately 12 dB lower [2]. The measurement setup for the 1.6-GHz chips [2] was similar to Fig. 7, with the exception of the use of two custom 1.6-GHz patch antennas rather than a power splitter and a commercially available patch antenna, and different analog filtering. For the 1.6-GHz signals, the heart signal was separated with analog filters before it was digitized. The first stage of analog filtering blocks the dc offset with a 0.03-Hz 12-dB/decade high-pass filter, avoids aliasing and removes out-of-band noise with a 10-Hz cutoff 12-dB/decade low-pass filter, and amplifies the signal 27 dB. The output from these analog filters is the "raw" data signal, which includes both respiration and heart information. This signal is then passed through a 1-Hz cutoff 12-dB/decade high-pass analog filter followed by a 1–3-Hz 6-dB/decade bandpass analog filter and amplified by 20 dB to isolate the heart movement from the respiration movement. This signal will be referred to as the

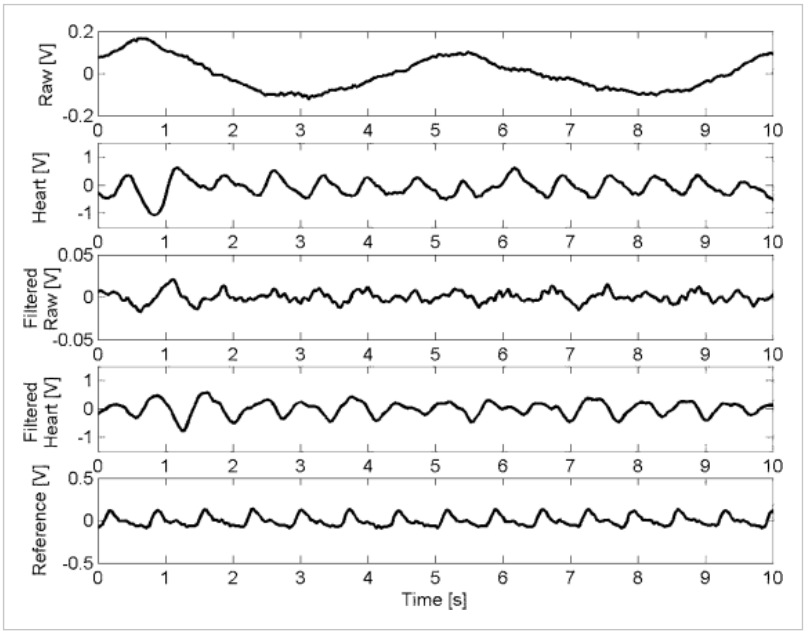

Fig. 11. Heart and respiration activity measured with the 1.6-GHz BiCMOS chip. The top trace is the analog-filtered raw signal, and the second is the analog-filtered heart signal. The third and fourth traces are the raw and heart signals, respectively, after digital filtering. The bottom trace is the reference obtained from the finger-pressure pulse sensor. The filtered heart signal was within one beat per minute of the reference 100% of the time, while the filtered raw signal agreed 92% of the time.

"heart" signal. The analog filtering for the 2.4-GHz signal had a high-pass cutoff frequency between that of the raw signal and that of the heart signal so both the raw and heart signals were passed through the digital filter for comparison. With all else equal, a signal passed through the analog filters used for the 2.4-GHz measurements would have accuracy between one passed through those used for the raw and those used for the heart 1.6-GHz measurements.

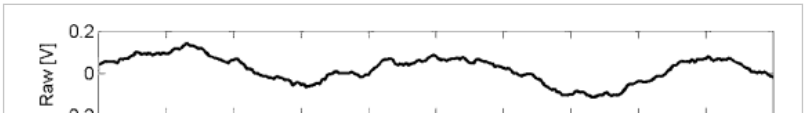

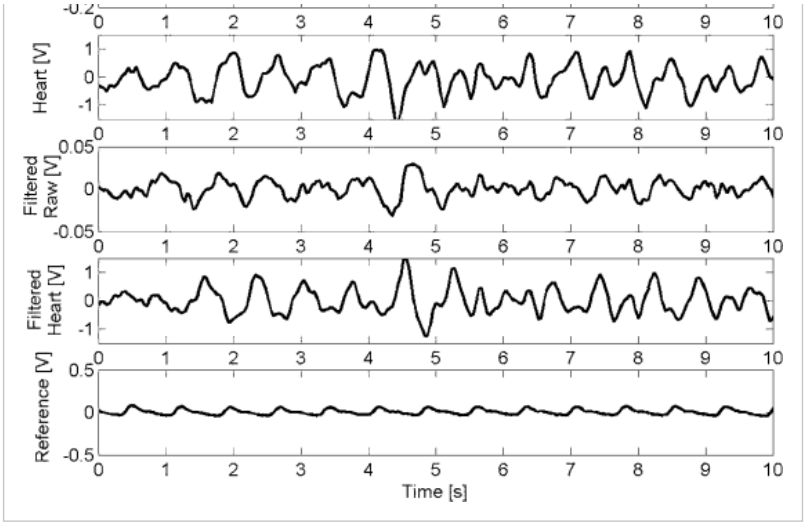

Fig. 12. Heart and respiration activity measured with the 1.6-GHz CMOS chip. The top trace is the analog-filtered raw signal and the second is the signal after analog heart filtering. The third and fourth traces are the raw and heart signals, respectively, after digital filtering. The bottom trace is the reference obtained from the finger-pressure pulse sensor. The filtered heart signal was within one beat per minute of the reference 98% of the time, while the filtered raw signal agreed 85% of the time.

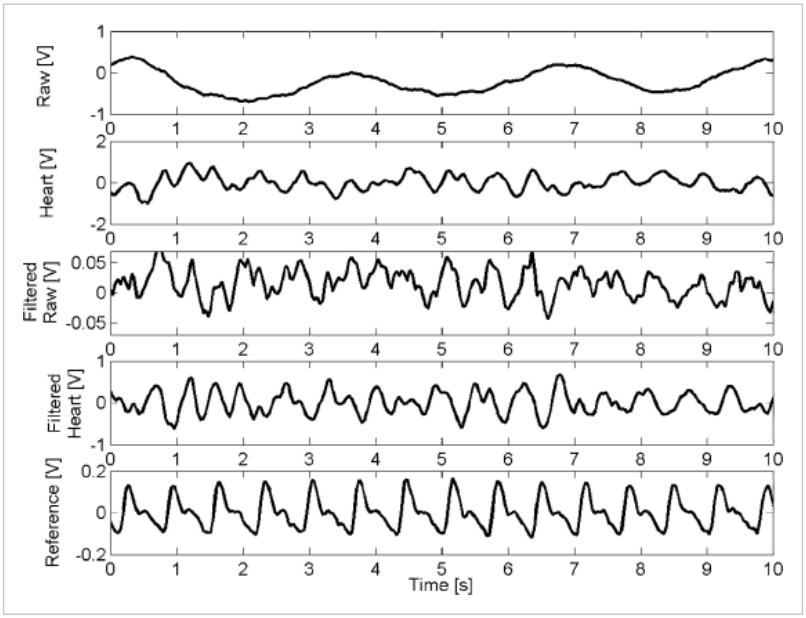

Fig. 13. Heart and respiration activity measured with the 1.6-GHz CMOS chip at a nonoptimal phase-demodulation point. The digitally filtered heart signal was within one beat per minute of the reference 44% of the time, while the digitally filtered raw signal agreed 33% of the time.

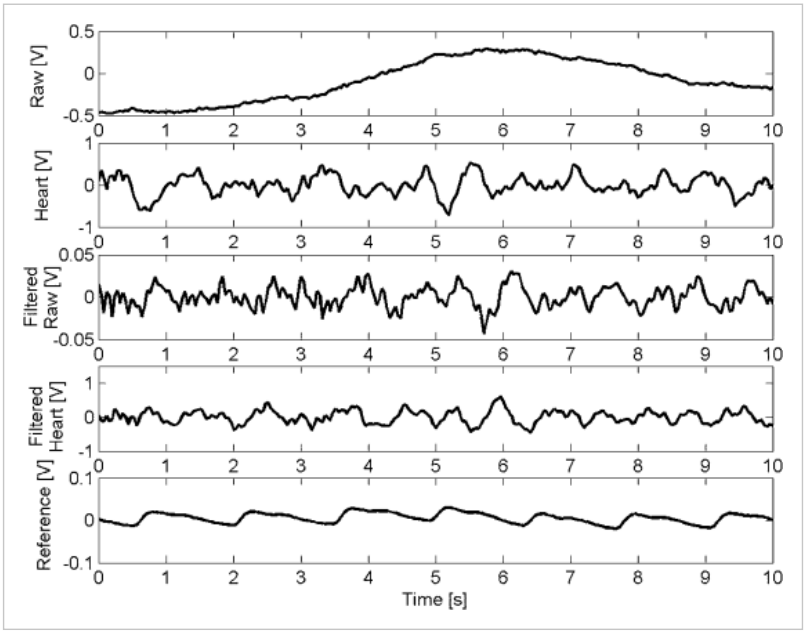

Fig. 14. Heart and respiration activity measured with the 1.6-GHz CMOS chip near the

optimum phase-demodulation point at a range of 85 cm rather than 50cm. The noise is significantly more pronounced than with a 50-cm range, and the accuracy is 52% for the digitally filtered raw signal and 63% for the digitally filtered heart signal.

In Fig. 11, after digital filtering, the heart signal from the BiCMOS chip was within one beat per minute of the reference 100% of the time, while the raw signal after digital filtering agreed with the reference 92% of the time. In Fig. 12, the digitally filtered heart signal from the CMOS chip was within one beat per minute of the reference 98% of the time, while the digitally filtered raw signal agreed 85% of the time. These measurements were made near the optimum phase-demodulation point. For comparison with measurements made with the 2.4-GHz chip at nonoptimal phase-demodulation points, a signal from the 1.6-GHz CMOS chip at a less ideal point is examined, and is shown in Fig. 13. In this signal, the digitally filtered heart signal was within one beat per minute of the reference 44% of the time, and the digitally filtered raw signal agreed 33% of the time. The 1.6-GHz BiCMOS chip has approximately 12-dB lower phase noise than the CMOS chips and, thus, using this chip, it is possible to obtain a clearer signal and to achieve a higher accuracy than with either CMOS chip. The two CMOS chips have comparable phase noise, and the heart-rate data obtained with those chips are of comparable quality. As shown in [2], using an external source with over 100-dB less phase noise than the BiCMOS oscillator increased the accuracy of detection by only 5%, indicating that it is not necessary to use high-quality oscillators for this application at a 50-cm range.

According to range-correlation theory (13), to operate at a greater range, a lower phase-noise source would be needed to achieve the same residual phase noise. Otherwise, with the same source, as range increases, the amount of noise at baseband will also increase. For example, at 85 cm, the 1.7 times increase in distance will result in a 4.6-dB increase in residual phase noise. Therefore, a source with at least 4.6 dB lower phase noise would be required to achieve the same results, assuming that residual phase noise is still the limiting factor. If the same source is used, the increase in residual phase noise is expected to adversely affect the heart-rate detection accuracy. As range increases, there is an additional factor of free-space loss and, therefore, a lower power received signal when the distance is increased, which will also affect the output signal. The effect of changing the target range was evaluated using the 1.6-GHz CMOS chip at the 85-cm range, and data are shown in Fig. 14. In this case, the heart-rate accuracy dropped to 63% from the 98% accuracy at a 50-cm range.

The difference in the heart-rate accuracy obtained with different levels of oscillator phase noise and with different target range confirms that residual phase noise is a limiting factor in this measurement system. Since the phase noise is such a factor, the range-correlation theory is important to consider in system engineering of a Doppler radar for vital-signs measurement. It implies the advantages of minimizing oscillator phase noise and of minimizing time delays. Keeping the antenna electrically close to the transceiver and keeping the target as close to the antenna as possible can reduce time delays, improving system performance. The baseband noise measurements at different phase points and the difference between the accuracy of the I and Q signals when one is at the null point emphasize the importance of avoiding the phase-demodulation null points, as the quadrature receiver does. When building a prototype monitoring device, a quadrature receiver will be used, and time delays will be minimized.

SECTION V.
Conclusion

Single-chip Doppler radars and their use in vital signs sensing have been described. The residual phase noise, which is a limiting factor in this system, depends on both the target range and oscillator phase noise. Free-running CMOS oscillators with -60 dBc/Hz phase noise at a 10-kHz offset were found to be adequate for heart-rate detection at distances up to 50 cm. Experimental verification of the range-correlation effect, which determines the level of residual phase noise, was presented, and the measured baseband noise spectrum agreed with theoretical values within an average of 5 dB. The benefit of a quadrature receiver in avoiding null points has been demonstrated. With a quadrature receiver, the lowest heart-rate accuracy was approximately 80%, a significant improvement over the lowest heart-rate accuracy of below 40% that was observed with a single receiver chain in a null point. With more advanced signal processing and further system integration, this chip could potentially be used as a home monitor for SIDS and OSAS. A prototype monitoring device, based on the quadrature chip, is currently being developed, and will be used for more extensive human testing.

ACKNOWLEDGMENT

The authors thank C. Metz and M. Budge for helpful discussions. The authors are grateful to Agere

The authors thank C. Fiets and M. Budge for helpful discussions. The authors are grateful to Agere Systems for chip fabrication and to Lucent Technologies for mentorship provided through the Graduate Research Program for Women. The authors further acknowledge and greatly appreciate M.Zierdt, J. Housel, and G. Meza for their assistance with board assembly and F. P. Hrycenko and T. Gabara for chip layout support.

Keywords

IEEE Keywords
Silicon, Doppler radar, Cardiology, Monitoring, CMOS technology, Phase noise, Semiconductor device measurement, Transceivers, BiCMOS integrated circuits, Microwave technology

INSPEC: Controlled Indexing
sleep, patient monitoring, biomedical equipment, biomedical electronics, cardiology, pneumodynamics, radar clutter, phase noise, radar applications, Doppler radar, CW radar, homodyne detection, radar detection, BiCMOS analogue integrated circuits, CMOS analogue integrated circuits

INSPEC: Non-Controlled Indexing
2.4 GHz, noncontact cardiopulmonary monitoring, single-chip silicon Doppler radar, range correlation, I/Q performance benefits, direct-conversion microwave Doppler-radar, Doppler-radar transceivers, CMOS analog integrated circuits, BiCMOS analog integrated circuits, phase-noise reduction, continuous-wave radar, homodyne detection, radar clutter, vital signs sensing, obstructive sleep apnea, 1.6 GHz

Authors

A.D. Droitcour
Dept. of Electr. Eng., Stanford Univ., CA, USA

Amy D. Droitcour (S'98) received the B.S. degree in electrical engineering (with honors) from Cornell University, Ithaca, NY, in 2000, the M.S. in electrical engineering from Stanford University, Stanford, CA in 2003, and is currently working toward the Ph.D. degree in electrical engineering at Stanford University.

Her research interests include biomedical applications of wireless technology.

Ms. Droitcour is a student member of the IEEE Microwave Theory and Techniques Society (IEEE MTT-S), the IEEE Solid State Circuits Society, and the IEEE Engineering in Medicine and Biology Society. She was the recipient of the Lucent Technologies/Bell Laboratories Graduate Research Fellowship. She received an honorable mention in the 2001 IEEE MTT-S International Microwave Symposium (IMS) Student Paper Competition, and was the first place recipient in the 2003 IEEE MTT-S IMS competition.

O. Boric-Lubecke

Olga Boric-Lubecke (S'90–M'90–SM'01) received the B.Sc. degree in electrical engineering from the University of Belgrade, Belgrade, Yugoslavia, in 1989, the M.S. degree in electrical engineering from the California Institute of Technology, Pasadena, in 1990, and the Ph.D. degree in electrical engineering from the University of California at Los Angeles, in 1995.

Prior to joining the Department of Electrical Engineering, University of Hawaii at Manoa, as an Associate Professor, she was a Member of the Technical Staff with Bell Laboratories, Lucent Technologies, Murray Hill, NJ, where she conducted research in RF integrated circuit

Lucent Technologies, Murray Hill, NJ, where she conducted research in RF integrated circuit technology and biomedical applications of wireless systems. From 1996 to 1998, she was a Visiting Research Scientist with the Institute of Physical and Chemical Research (RIKEN), Sendai, Japan. From 1995 to 1996, she was a Resident Research Associate with the NASA Jet Propulsion Laboratory, Pasadena, CA. Her current research interests include silicon RF integrated circuits, high-frequency integrated circuits, and biomedical applications.

Prof. Boric-Lubecke serves on Technical Program and Steering Committees for various IEEE and SPIE symposia. She was the corecipient of the 2001 IEEE Microwave Theory and Techniques Society (IEEE MTT-S) Best Student Paper Honorable Mention Award, the 2001 IEEE Engineering in Medicine and Biology Society (IEEE EMBS-S) Best Student Paper Third Place Award, and the 2003 IEEE MTT-S Best Student Paper First Place Award.

V.M. Lubecke

Victor M. Lubecke (S'86–M'86–SM'98) received the B.S. degree in electrical and electronics engineering from the California State Polytechnic University, Pomona, in 1986, and the M.S. and Ph.D. degrees in electrical engineering from the California Institute of Technology, Pasadena, in 1990 and 1995, respectively.

Prior to joining the Department of Electrical Engineering, University of Hawaii at Manoa, as an Associate Professor, he was with Bell Laboratories, Lucent Technologies, where his research focused on microelectromechanical systems (MEMS) technologies for wireless and optical communications, and monitoring technologies for biomedical and industrial applications. From 1987 through 1996, he was with the NASA Jet Propulsion Laboratory. From 1996 to 1998, he was with the Institute for Physical and Chemical Research (RIKEN), Sendai, Japan, where his research involved various aspects of MEMS and terahertz technologies for space communications and remote-sensing applications.

Prof. Lubecke serves on Technical Program and Steering Committees for various IEEE and SPIE symposia. He was the recipient of the 2000 Microwave Prize for Best Paper presented at the Asia–Pacific Microwave Conference. He was corecipient of the 2003 First Prize for Best Student Paper of the IEEE Microwave Theory and Techniques Society (IEEE MTT-S) International Microwave Symposium (IMS), the Third Prize for a student paper at the 2001 International Conference of the IEEE Engineering in Medicine and Biology Society (IEEE EMBS-S), and Honorable Mention for a student paper at the 2001 IEEE MTT-S IMS.

J. Lin

Jenshan Lin (S'91–M'94–SM'00) received the B.S. degree from the National Chiao Tung University, Hsinchu, Taiwan, R.O.C., in 1987, and the M.S. and Ph.D. degrees in electrical engineering from the University of California at Los Angeles (UCLA), in 1991 and 1994, respectively. His doctoral dissertation concerned active integrated antenna and spatial power combining.

In 1994, he joined AT&T Bell Laboratories (later Lucent Bell Laboratories), Murray Hill, NJ, as a Member of Technical Staff. He became the Technical Manager of RF and High Speed Circuit Design Research in 2000. Since joining Bell Laboratories, he has been involved with integrated circuits using different technologies for different applications, including 30-GHz InP HBT voltage-controlled oscillators (VCOs) for local multipoint distribution systems (LMDSs), fully integrated low phase-noise BiCMOS VCOs for global system for mobile communications (GSM) receivers, high-${ Q}$ inductors, chip-package co-design with advanced flip-chip packages, and low-noise high-linearity CMOS RF integrated circuits (RFICs). He led the Bell Laboratories' Base Station RFIC team to demonstrate the first low-cost high-performance silicon CMOS RFIC solution for wireless base stations, which was press released at the International Solid-State Circuits Conference (ISSCC) in 2001. In

press released at the International Solid-State Circuits Conference (ISSCC), in 2004. In September 2001, he joined Agere Systems, a spin-off from Lucent, and was involved with high-speed CMOS circuit design for 10-G/40-G broad-band communications. In July 2003, he joined University of Florida, Gainesville, where he is currently an Associate Professor. He has authored or coauthored over 80 technical publications and invited talks in international conferences and journals. He holds five patents. His current research interests include RF system-on-chip integration, high-speed broad-band circuits, wireless sensors, and self-adaptive transceivers.

Dr. Lin has actively participated in the IEEE Microwave Theory and Techniques Society (IEEE MTT-S) and currently serves on the IEEE MTT-S Administrative Committee and Wireless Technology Committee. He also serves on other conference committees including the IEEE MTT-S International Microwave Symposium (IMS), RFIC, and RAWCON. He served on the 2003 IEEE MTT-S IMS Steering Committee, the 2001 Sarnoff Symposium Technical Program Committees, the 1998 and 2000 Chip-Package Co-Design Workshop, and the 1999 IC/Package Design Integration Symposium. He was the recipient of the 1994 UCLA Outstanding Ph.D. Award and the 1997 Eta Kappa Nu Outstanding Young Electrical Engineer Honorable Mention Award.

G.T.A. Kovacs

Gregory T. A. Kovacs (M'83) received the BA.Sc. degree in electrical engineering from the University of British Columbia, Victoria, BC, Canada, in 1984, the M.S. degree in bioengineering from the University of California at Berkeley, in 1985, and the Ph.D. degree in electrical engineering and the MD degree from Stanford University, Stanford, CA, in 1992, respectively.

He possesses extensive industry experience including co-founding several companies, most recently, Cepheid, Sunnyvale, CA. He is an Associate Professor of electrical engineering with Stanford University with a courtesy appointment in the Department of Medicine. In addition, he is the Director of Medical Device Technologies for the Astrobionics Program of the NASA Ames Research Center, and for the Stanford–NASA National Biocomputation Center. He helps direct a variety of projects spanning wearable physiologic monitors, biosensor instruments for detection of chemical and biological warfare agents and space biology applications, and free-flyer experiment payloads. He served as the Investigation Scientist for the debris team of the Columbia Accident Investigation Board, having worked for the first four months after the accident at the Kennedy Space Center, FL. In this role, he carried out physical, photographic, X-ray, chemical, and other analyses on selected items from the nearly 90 000 lb of recovered debris and worked toward understanding the nature of the accident. His current research interests include biomedical instruments and sensors, miniaturized spaceflight hardware, and biotechnology.

Dr. Kovacs is a long-standing member of the Defense Sciences Research Council (DARPA) and has served as an associate chair and chairman. He is a Fellow of the American Institute for Medical and Biological Engineering. He held the Noyce Family Chair and was a Terman and then University Fellow at Stanford University. He was the recipient of a National Science Foundation (NSF) Young Investigator Award.

Related Articles

A wireless, passive carbon nanotube-based gas sensor
Keat Ghee Ong; Kefeng Zeng; C.A. Grimes

Competitive learning with floating-gate circuits
D. Hsu; M. Figueroa; C. Diorio

State of the art in sensor technologies for sewer inspection
O. Duran; K. Althoefer; L.D. Seneviratne

Ultra low phase noise sapphire-SiGe HBT oscillator
O. Llopis; G. Cibiel; Y. Kersale; M. Regis; M. Chaubet; V. Giordano

Hydrogen catalytic oxidation reaction on Pd-doped porous silicon
C. Tsamis; L. Tsoura; A.G. Nassiopoulou; A. Travlos; C.E. Salmas; K.S. Hatzilyberis; G.P. Androutsopoulos

Integrated LC oscillators for frequency synthesis in wireless applications
C. Samori; S. Levantino; A.L. Lacaita

OpenRAN: a new architecture for mobile wireless Internet radio access networks
J. Kempf; P. Yegani

A tool to coordinate tools
R. Bisiani; F. Lecouat; V. Ambriola

An Internet-based system for the commerce of medical devices. A portal for improving communication between healthcare professionals and the medical device industry
S. Palamas; D. Kalivas; O. Panou-Diamandi

GSM over Ethernet
R. Dettmer